J. Fluid Mech. (1983), *vol.* 130, *pp.* 347–376
Printed in Great Britain

Thermocapillary convection in a rectangular cavity: asymptotic theory and numerical simulation

By M. STRANI, R. PIVA AND G. GRAZIANI
Istituto di Meccanica Applicata, Università di Roma, Rome, Italy

(Received 13 April 1982 and in revised form 4 January 1983)

The steady motion of a Newtonian fluid in a rectangular enclosure open on its upper side is considered under the action of thermocapillary forces due to surface-tension gradients along the free surface. An asymptotic solution, in the limiting case of the aspect ratio $A \to 0$, is found and discussed for the cases where the surface deformation may be neglected, that is for contact angles at the lateral walls equal to $\frac{1}{2}\pi$ and very small values of the crispation number. The flow field has also been analysed in a wide range of the governing parameters A, Mg, Cr, by a computational model particularly appropriate to simulate free-surface flows. For $A \ll 1$ the numerical results confirm the behaviour predicted by the asymptotic theory, while for $A \geqslant 1$ several characteristic features of the flow-field structure are emphasized. For increasing Mg, the surface layer under the free surface maintains in the mid-section a constant value, dependent only on A, and decreases together with the thermal boundary-layer thickness near the lateral walls. For increasing A, the motion remains confined in a region near the free surface; hence the overall Nu, starting from the pure conduction value ($Nu \to 1$ as $A \to 0$) inccreases with A, reaching a maximum, to tend again to unity as $A \to \infty$. The surface deformation, at least for very small values of the crispation number, seems to have a negligible influence on the qualitative aspects of the flow-field structure.

1. Introduction

Thermocapillary convection, driven by surface-tension gradients, may be generated in an open rectangular cavity with differentially heated lateral walls by the temperature gradients occurring at the free surface.

These flows, known as Marangoni flows, are, in general, intrinsically coupled with convective flows driven by the buoyancy forces that originate from the same temperature gradients.

Therefore thermocapillary convection is rarely found by itself, even in those technological applications where its presence is more relevant, as in microgravity conditions, e.g. material processes in space (Ostrach 1982) or in fields of very small dimensions, e.g. crystal-growth melts (Schwabe 1981). However, while for natural convection a satisfactory understanding of the flow-field structure in its various regimes has been reached in many studies (Gill 1966; Cormack, Leal & Imberger 1974*a*; Cormack, Leal & Seinfeld 1974*b*), for thermocapillary convection a systematic analysis is still missing and phenomena occurring in a wide range of the relevant characteristic parameters (aspect ratio, Marangoni, Prandtl and crispation numbers) need to be interrelated to give a self-consistent representation of the flow.

Most of the experimental investigations (Schwabe, Scharmann & Preisser 1979; Schwabe & Scharmann 1981; Chun 1980; Chun & Wuest 1978) trying to emphasize thermocapillary convection have been performed in small-dimension fields with

ground-level gravity force and large bulk temperatures, that is in conditions for which natural convection and free-surface radiation may give a significant contribution. The few experiments actually conducted in reduced gravity, as existing in orbiting spacecraft (Bourgeois & Brasheors 1977), or during free fall in a drop tower (Ostrach & Pradhan 1978), apart from confirming the importance of Marangoni flows, are not substantiated by measurements that give information about the peculiar features of the flow field. Though the assumption of zero gravity does not imply any further difficulty, numerical solutions (Chang 1978; Chang & Wilcox 1976; Clark & Wilcox 1980) are in general devoted to combined convection problems, with the aim of simulating real conditions for comparison with experimental results. In these studies attention is mainly paid to the generation of the overall recirculations without specific interest in the critical regions near the walls, and the transition, at larger Marangoni numbers, to a boundary-layer regime.

Thermocapillary convection has been isolated in the present study to analyse the influence of the characteristic parameters on the flow field. The analytical results, obtained through an asymptotic theory in §3, describe the behaviour of the flow field when Cr is very small, for values of the aspect ratio $A \ll 1$ and arbitrary values of the Reynolds number. The flow region is separated into a core region and two endwall regions, where asymptotic expansions of the unknown variables in powers of the aspect ratio A are assumed. A first approximation of the free-surface configuration is also given, together with an appropriate evaluation of the range of the various non-dimensional parameters for which the results of the asymptotic theory may be of practical use.

The asymptotic solutions and the physical trends discussed in §3 are confirmed by the numerical results described in §4, which have been obtained by a computational model based on finite differences in curvilinear coordinates fitting the free-surface deformation. The wider investigation, performed through the numerical simulation, for values of the parameters outside of the range required by the asymptotic theory, led to a systematic collection of results, which have been critically analysed and correlated to formulate, in §5, a tentative description of the flow-field structure in its different regimes.

2. Mathematical formulation

The steady plane flow field of an incompressible Newtonian fluid (+) in a rectangular enclosure open on its upper side (figure 1) is considered. The interface $y' = H'(x')$ which separates fluid (+) from fluid (−), is an unknown of the problem, to be determined together with the field-dependent variables.

The two lateral walls are kept at different temperatures T'_c and T'_w, while the bottom of the enclosure is assumed to be thermally insulated. In these conditions ($T'_c \neq T'_w$) a convective motion is induced, in general, under the combined action of buoyancy (natural convection) and the shear stress exerted at the free boundary by a temperature-induced surface-tension gradient along the interface itself (thermocapillary convection). The relative importance of these two types of convection may be estimated by the value of the modified Bond number $\overline{Bo}$, that is the ratio between the Grashof number Gr and the Marangoni number Ma (Ostrach & Pradhan 1978).

A general mathematical model for the coupled motion of the bulk and the surface phases has been presented previously (Bedaux, Albano & Mazur 1976; Napolitano 1978) and expressed in general tensor form (Strani & Piva 1982) to allow the use of curvilinear non-orthogonal coordinates. In fact these coordinates are more suitable to fit all the boundaries, in particular the free surface, to obtain more accurate

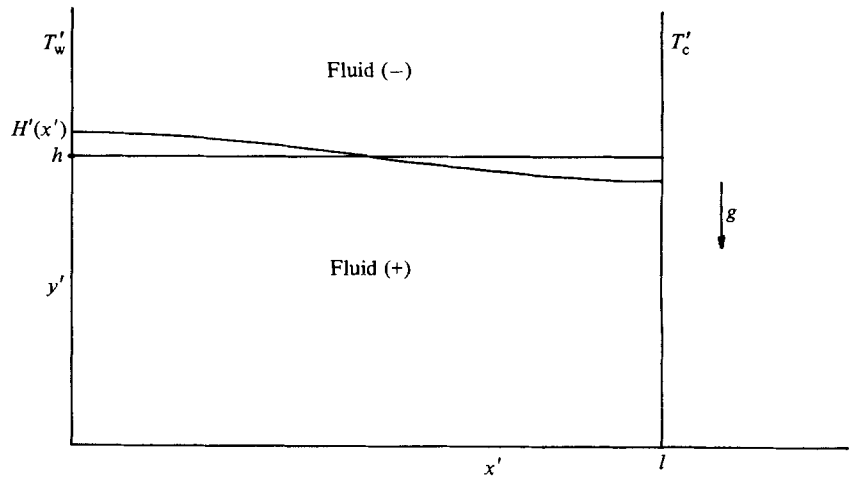

FIGURE 1. Sketch of the geometrical configuration of the problem.

numerical solutions. The main simplifying hypotheses on which the present study is based are now explicitly discussed. A zero modified Bond number, which is physically acceptable in a microgravity environment or for very small linear dimensions of the cavity, has been assumed in order to isolate thermocapillary convection, as previously discussed. The thermal and mechanical effects of the fluid (−) on the interface phase are assumed to be negligible, with the exception of a constant known pressure. This hypothesis is approximately valid, for instance, when the fluids (+) and (−) are respectively a liquid and a gas. Consequently the motion of fluid (+) is considered to be under the influence of only the forces exerted by the interface layer.

Continuous values, between the bulk and the surface phases, of velocity and temperature at the free surface are assumed, together with zero values of the surface thermal conductivity and viscosity. The abovementioned general mathematical model gives an opportunity to account for discontinuities in the values of velocity and temperature at the interface, as well as for the existence of dissipative processes on the interface, while the asymptotic theory presented in this paper could be easily developed under these more general conditions. Numerical evidence has shown (Piva, Strani & Graziani 1981), however, that the main features of the flow-field structure are scarcely affected by these last assumptions. The resulting gain in simplicity is therefore favourable for this first study on the flow-field structure. The non-dimensional form of the Navier–Stokes equations and boundary conditions that follow from the complete system, after the above assumptions, are as follows:

$$u^k_{|k} = 0 \quad \text{mass balance,} \tag{2.1}$$

$$(u^h u^k - \sigma^{hk})_{|k} = 0 \quad \text{momentum balance,} \tag{2.2}$$

$$(u^k T - q^k)_{|k} = 0 \quad \text{thermal-energy balance,} \tag{2.3}$$

where u^k are contravariant components of the velocity, the Eckert number has been assumed to be negligible and the heat flux q^k, and stess tensor σ^{hk} are given by the constitutive equations

$$q^k = -\frac{1}{Re\,Pr} g^{hk} T_{,h} \tag{2.4a}$$

$$\sigma^{hk} = -pg^{hk} + \frac{1}{Re}(u_{n|m} + u_{m|n})\, g^{hn} g^{km}, \tag{2.4b}$$

where p is the pressure. The metric-tensor components g^{hk} and the Christoffel symbols appearing in the covariant derivatives may be easily derived by a singled-valued continuous and differentiable map

$$x^2 = \frac{x'}{l} = x^2(\xi^2, \xi^3), \tag{2.5a}$$

$$x^3 = \frac{y'}{h} = x^3(\xi^2, \xi^3), \tag{2.5b}$$

which defines a system of generalized coordinates $\langle \xi^k \rangle$ (Latin indices run from 2 to 3) in the physical plane normal to the axis x^1, where the interface coincides with a portion of the coordinate plane $\xi^3 = 1$ (see figure 1). Different lengthscales l and h have been assumed respectively for the x' and y' directions, and the aspect ratio is defined as $A = h/l$. The Reynolds number Re and Prandtl number Pr that appear in the above system of equations are defined by

$$Re = \left|\frac{\mathrm{d}\sigma'}{\mathrm{d}T'}\right| \frac{(T'_{\mathrm{w}} - T'_{\mathrm{c}})\rho h}{\mu^2}, \quad Pr = \frac{\mu c_p}{\lambda}, \tag{2.6}$$

where ρ is the density, σ' the surface tension, and μ and λ are viscosity and thermal diffusivity coefficients. The reference velocity in Re has been specified, following Ostrach (1982), by the driving mechanism of the flow at the free surface:

$$U'_{\mathrm{r}} = \left|\frac{\mathrm{d}\sigma'}{\mathrm{d}T'}\right| \frac{(T'_{\mathrm{w}} - T'_{\mathrm{c}})}{\mu} \frac{h}{l}. \tag{2.7}$$

We will discuss later in §5 the range of validity of this choice, which seems to be more extended than originally proposed by Ostrach. The resulting expression of the Reynolds number is often indicated in the literature as 'surface-tension Reynolds number' while its product times Pr is usually called the Marangoni number Ma. The boundary conditions at the free surface $\zeta^3 = 1$ are

$$u^3 = 0, \tag{2.8a}$$

$$\frac{\sigma^{33}}{g^{33}} + \frac{1}{Re}\sigma b_2^2 = 0, \tag{2.8b}$$

$$\frac{\sigma}{(g^{33})^{\frac{1}{2}}} + \frac{1}{Re}\sigma_{,2} = 0, \tag{2.8c}$$

$$q^3 = 0, \tag{2.8d}$$

where the curvature-tensor component b_2^2 is given by the inverse of the local radius curvature of the free surface. The surface tension σ is assumed to be given by the linear relation in temperature

$$\sigma = \frac{1}{Cr} - T \tag{2.9}$$

where the crispation number Cr is given by

$$Cr = \left|\frac{\mathrm{d}\sigma'}{\mathrm{d}T'}\right| \frac{T'_{\mathrm{w}} - T'_{\mathrm{c}}}{\sigma'(T'_{\mathrm{c}})}. \tag{2.10}$$

Finally the following boundary conditions hold at the fixed solid boundaries:

$$u^2 = u^3 = 0, \quad T_{,3} = 0 \quad (\xi^3 = 0), \tag{2.11a}$$

$$u^2 = u^3 = 0, \quad T = \xi^2 \quad (\xi^2 = 0, 1). \tag{2.11b}$$

3. Asymptotic solution

The free-surface shape $H'(x')$ and, with it, the integration domain $\mathscr{D}$ have to be considered as unknowns in the solution of a thermocapillary-flow problem in a bounded region.

Since, in the limit $Cr \to 0$, the free-surface shape has the trivial solution $H'(x') = h$ and $\mathscr{D} \equiv \mathscr{D}_0 \equiv \{(x_0, y_0) | 0 \leqslant x_0 \leqslant 1,\ 0 \leqslant y_0 \leqslant h\}$, profitable use can be made, in the general case $Cr \neq 0$, of the domain perturbation method (Joseph & Fosdick 1972), whose main features, when applied to the present case, are here briefly recalled.

Under the group of hypotheses mentioned in §2, the governing bulk conservation equations (2.1)–(2.3) become, when reference is made to a Cartesian system of coordinates,

$$Auu_{,x} + vu_{,y} = (A\,Re)^{-1}(-Ap_{,x} + A^2 u_{,xx} + u_{,yy}), \tag{3.1}$$

$$Auv_{,x} + vv_{,y} = (A\,Re)^{-1}(-p_{,y} + A^2 v_{,xx} + v_{,yy}), \tag{3.2}$$

$$Auu_{,x} + v_{,y} = 0, \tag{3.3}$$

$$AuT_{,x} + vT_{,y} = (A\,Re\,Pr)^{-1}(A^2 T_{,xx} + T_{,yy}) \tag{3.4}$$

in $\mathscr{D} \equiv \{(x, y) | 0 \leqslant x \leqslant 1,\ 0 \leqslant y \leqslant H(x)\}$, while from (2.8)–(2.11) the following boundary conditions result:

$$T = 0, \quad u = v = 0 \quad (x = 0, 1), \tag{3.5a}$$

$$T_{,y} = 0, \quad u = v = 0 \quad (y = 0), \tag{3.5b}$$

$$\left.\begin{aligned} &-AuH_{,x} + v = 0, \\ &-AH_{,x}(2Au_{,x}) + (1 - 2A^2 H_{,x}^2)(u_{,y} + Av_{,x}) + 2AH_{,x} v_{,y} \\ &\qquad = (T_{,x} + H_{,x} T_{,y})(1 + A^2 H_{,x}^2)^{\frac{1}{2}}, \\ &-A^2 H_{,x} T_{,x} + T_{,y} = 0 \end{aligned}\right\} \quad (y = H(x)). \tag{3.5c}$$

The remaining boundary condition at $y = H(x)$ gives the differential equation for the free-surface shape

$$\begin{aligned} -p + (1 + A^2 H_{,x}^2)^{-1}[2A^3 H_{,x}^2 u_{,x} - 2AH_{,x}(u_{,y} + Av_{,x}) + 2v_{,y}] \\ = (Cr^{-1} - T)\,AH_{,xx}(1 + A^2 H_{,xx}^2)^{-\frac{3}{2}}, \end{aligned} \tag{3.5d}$$

to be solved with the boundary conditions

$$H_{,x} = 0 \quad (x = 0, 1), \tag{3.5e}$$

and the condition on the total-volume conservation

$$\int_0^1 H(x)\,\mathrm{d}x = 1. \tag{3.5f}$$

An analytical dependence on crispation number of the unknown functions of the

free-boundary problem under consideration is assumed. The one-to-one map

$$x = x_0, \quad y = y_0 H(x_0, Cr) \tag{3.6}$$

between the integration $\mathscr{D}$ and the reference domain $\mathscr{D}_0$ is considered.

The unknown vector of the free-boundary problem, when evaluated in $\mathscr{D}_0$ through the map (3.6), is expanded in the parameter Cr according to

$$\begin{vmatrix} u(x_0, y_0, Cr) \\ v(x_0, y_0, Cr) \\ p(x_0, y_0, Cr) \\ T(x_0, y_0, Cr) \\ H(x_0, Cr) \end{vmatrix} = \sum_n \begin{vmatrix} u^{[n]}(x_0, y_0) \\ v^{[n]}(x_0, y_0) \\ p^{[n]}(x_0, y_0) \\ T^{[n]}(x_0, y_0) \\ H^{[n]}(x_0, y_0) \end{vmatrix} Cr^n. \tag{3.7}$$

By substituting (3.7) into (3.1)–(3.5), an infinite sequence of differential equations and boundary conditions for the unknowns, given by the 'total' nth derivatives $(\ )^{[n]}$ with respect to Cr at $Cr = 0$ keeping x_0, y_0 fixed, is found.

3.1. *Asymptotic solution* $(A \to 0)$ *for the zeroth-order expansion in Cr*

By a straightforward application of the domain perturbation method, one obtains, at the zeroth order,

$$H^{[0]} = 1,$$

while $u^{[0]}$, $v^{[0]}$, $p^{[0]}$, $T^{[0]}$ are found to satisfy a system of differential equations and boundary conditions which are the limit, as $H_{,x} \to 0$, of (3.1)–(3.5).

After the positions (hereinafter the superscript $(\ )^{[0]}$ is dropped for the zeroth-order solution)

$$u = \psi_{,y}, \quad v = -A\psi_{,x}, \tag{3.8}$$

$$-\omega = A^2\psi_{,xx} + \psi_{,yy}, \tag{3.9}$$

this may be written as

$$\psi_{,y}\omega_{,x} - \psi_{,x}\omega_{,y} = \frac{1}{A^2 Re}(A^2\omega_{,xx} + \omega_{,yy}), \tag{3.10}$$

$$\psi_{,y}T_{,x} - \psi_{,x}T_{,y} = \frac{1}{A^2 Re\, Pr}(A^2 T_{,xx} + T_{,yy}), \tag{3.11}$$

with the boundary conditions

$$T = x, \quad \psi = \psi_{,x} = 0 \quad (x = 0, 1), \tag{3.12a}$$

$$T_{,y} = 0 \quad (y = 0, 1), \tag{3.12b}$$

$$\psi_{,y} = 0 \quad (y = 0), \tag{3.12c}$$

$$\psi_{,yy} = -T_{,x} \quad (y = 1). \tag{3.12d}$$

The problem (3.10)–(3.12), in the limiting case $A \to 0$ with both Reynolds and Prandtl numbers fixed, is analysed by the standard method of matched asymptotic expansions, following the procedure successfully applied to the study of natural convection in closed enclosures by Cormack *et al.* (1974*a*).

Equations (3.10)–(3.12) in the limit $A \to 0$ have a solution for the stream function ψ which cannot satisfy the boundary conditions (3.12*a*) near the endwalls. It can

therefore be expected that, as $A \to 0$, a central region (core) develops, bounded by two regions near $x = 0$ and $x = 1$ where the structure of the flow field is different. This assumption is moreover confirmed by the numerical results (presented in §4), showing that, for small values of the aspect ratio, a core region, where the streamlines are nearly parallel to the x-axis, exists. A substantial deviation from this structure only occurs near the vertical endwalls in regions whose lengthscale is $O(h)$.

The asymptotic solution for the velocity and temperature field in the core and the end regions will be separately analysed and successively composed by use of the standard method of matched asymptotic expansions. In both regions the following simple expansions of the solutions in powers of A will be assumed:

$$\psi = \psi_k A^k, \quad \omega = \omega_k A^k, \quad T = T_k A^k, \tag{3.13}$$

where $k = 0, 1, 2, \ldots$ and the summation convention over repeated indices holds. The solution method presented below, although independently developed by the authors, turns out to be a particular case, for $Cr = 0$, of the method recently proposed by Sen & Davis (1982). Therefore reference is made, when possible, to their work.

3.1.1. *The flow in the core region.* By substituting the expansions (3.13) of the field variables into (3.9)–(3.11) and into the boundary conditions (3.12*c*, *d*) and, by equating terms of the same order in A, a similar form of the functions ψ and T in the core is obtained for each k:

$$\psi = K_1(\tfrac{1}{4}y^2 - \tfrac{1}{4}y^3), \tag{3.14}$$

$$T = K_1 x - (K_1 A)^2 Re\, Pr(\tfrac{1}{16}y^4 - \tfrac{1}{12}y^3) + K_2, \tag{3.15}$$

where

$$K_1 = c_k A^k, \tag{3.16}$$

$$K_2 = b_k A^k, \tag{3.17}$$

and c_k, b_k are constants (depending on Re and Pr) to be determined, as shown below, through asymptotic matching with the solution near the endwall. Equations (3.14) and (3.15) coincide, when $A = 0$, with equations (3.5) and (3.6) of Sen & Davis (1982).

An $O(1)$ approximation of the temperature in the core does not depend on y, and, since $c_0 = 1$ (3.21*c*), the temperature drop occurs essentially across the core. In the present asymptotic solution the heat transfer is hence dominated by pure conduction. It must be pointed out that this is not due to a 'pure conduction' limit with A fixed and $Re \to 0$, but is achieved for $A \to 0$, with arbitrary but fixed values of Re.

The $O(1)$ solution (3.14), (3.15) for the flow field in the core is immediately recognized to be coincident with the one proposed by Levich (1962). The substitution of (3.14) into the bulk momentum-conservation equations, gives

$$p_{,x} = -\frac{3}{2}\frac{K_1}{A}, \quad p_{,y} = 0. \tag{3.18}$$

The $O(1)$ approximation of (3.18) gives the longitudinal pressure gradient, not explicitly formulated by Levich. The resulting jump of pressure across the free surface is balanced by a curvature of the free surface that tends to zero as $Cr \to 0$ (see (3.5*d*)).

The above observation overcomes the criticism expressed by Yih (1968) with regard to the Levich solution.

A further comment on the adequacy of Levich's approximate solution can be made. As will be shown below, the first correction to the $O(1)$ value $K_1 = 1$ is $O(A^3)$. Therefore Levich's solution is a good approximation of the flow field in the core, as

$Cr \to 0$, even if account is taken of a relatively small amount of convection in the heat-transfer process. In fact (3.14), (3.15) show that the convective heat flux in the longitudinal direction is exactly balanced, at $O(A^2)$, by the onset of conduction in the y-direction, while, at the same order, the velocity flow field and the longitudinal temperature gradient are not modified with respect to the $O(1)$ approximation.

Finally a remark has to be made on the different features between the present asymptotic theory for $A \to 0$, Re fixed and the solution for A fixed and $Re \to 0$. In the present case the temperature drop occurs essentially across the core region, while in the end regions the flow is simply turned through 180° as required by the boundary conditions on the lateral walls. On the other hand, the numerical results of §4 indicate that, for A fixed and increasing values of Re, nearly all the temperature drop occurs in two thin layers near the endwalls, mainly near the cold wall, which thus provide the driving force for the flow, while the core ensures the inflow–outflow from the lateral boundary layers.

3.1.2. *The flow near the endwalls.* The coefficients c_k, b_k of the core solution are evaluated through the matching of the core solution (3.14), (3.15) with the asymptotic solutions near the end walls. The development of these solutions gives moreover an opportunity of discussing some interesting features of thermocapillary flows.

In agreement with the above considerations, no boundary-layer region near the endwalls exists: consequently the characteristic lengthscales in each direction are $O(h)$, and the proper non-dimensional variable for the longitudinal direction is

$$\xi = \frac{x}{A} \quad \text{near the cold wall,} \tag{3.19a}$$

$$\xi = \frac{1-x}{A} \quad \text{near the warm wall,} \tag{3.19b}$$

while, instead of the temperature, it is convenient to make use of the variables

$$\theta^{\mathrm{c}}(\xi, y) = T(\xi, y) \quad \text{near the cold wall,} \tag{3.20a}$$

$$\theta^{\mathrm{w}}(\xi, y) = 1 - T(\xi, y) \quad \text{near the warm wall.} \tag{3.20b}$$

As for the core region, the simple expansions (3.13) of the unknown functions ψ, ω, θ are assumed to be valid. By substituting these expansions into (3.10)–(3.12), and by equating terms of the same order in A, an infinite sequence of differential equations and boundary conditions for the unknown functions ψ_k, ω_k, θ_k is obtained. Since the method of solution strictly follows the one applied to natural convection by Cormack *et al.* (1974), and the set of differential equations and boundary conditions may be found as a particular case, for $Cr = 0$, of the corresponding ones presented by Sen & Davis (1982) we omit them here (for further details see Strani *et al.* 1982). It is however worthwhile listing here the main results of our analysis. In particular the decomposition of the flow-field variables at the various orders and their quantitative evaluation up to $O(A^3)$ – introduced by Cormack *et al.* (1974) for the natural convection problem and not considered by Sen & Davis (1982) – is the basis for the subsequent discussion on the trends of the flow field at increasing Re.

At $O(1)$

$$\theta_0^{\mathrm{c}} = \theta_0^{\mathrm{w}} = 0, \tag{3.21a}$$

$$\psi_0^{\mathrm{c}} = \psi_0^{\mathrm{w}} = \psi_0(\xi, y), \tag{3.21b}$$

$$c_0 = 1, \quad b_0 = 0. \tag{3.21c}$$

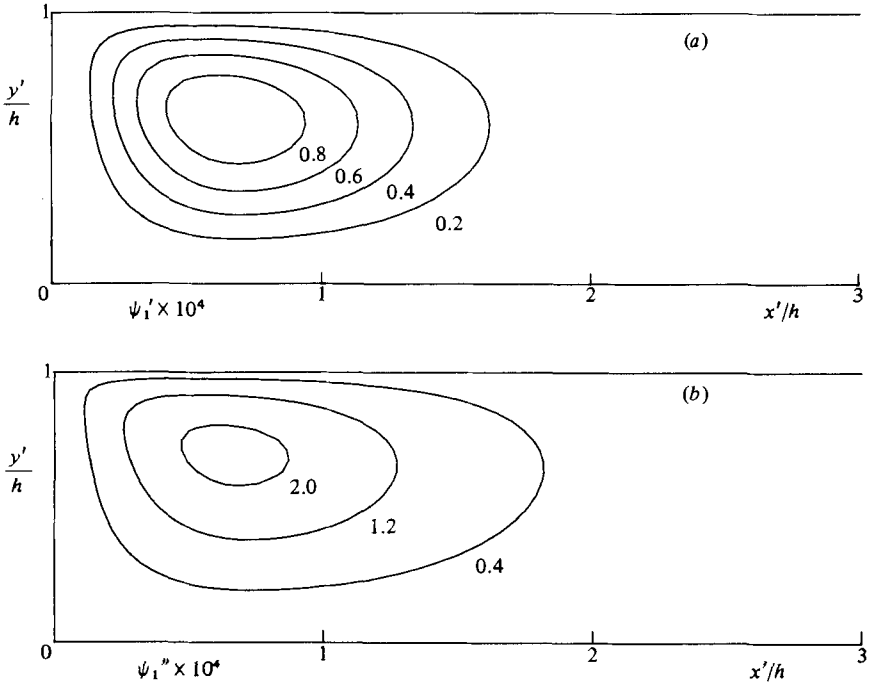

FIGURE 2. $O(A)$ correction on stream function: streamlines.

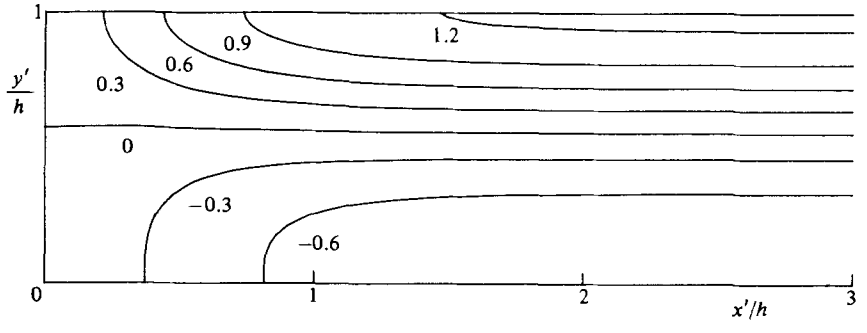

FIGURE 3. $O(A^2)$ temperature correction $\theta_2' \times 10^2$: isotherms.

The field $\psi_0(\xi, y)$ has been evaluated numerically. The streamline plot, as it is identical with the one presented in figure 3 of Sen & Davis (1982), is here omitted.

At $O(A)$

$$\theta_1^{\mathrm{c}} = \theta_1^{\mathrm{w}} = \xi, \tag{3.22a}$$

$$\psi_1^{\mathrm{c}} = -\psi_1^{\mathrm{w}} = \psi_1(\xi, y) = Re\,\psi_1' + Re\,Pr\,\psi_1'', \tag{3.22b}$$

$$c_1 = b_1 = 0. \tag{3.22c}$$

The functions ψ_1', θ_2' are found numerically, and the corresponding streamlines are plotted in figures 2(*a–b*).

Both corrections, of the same order of magnitude, give rise to a set of counter-clockwise closed streamlines located near the endwalls.

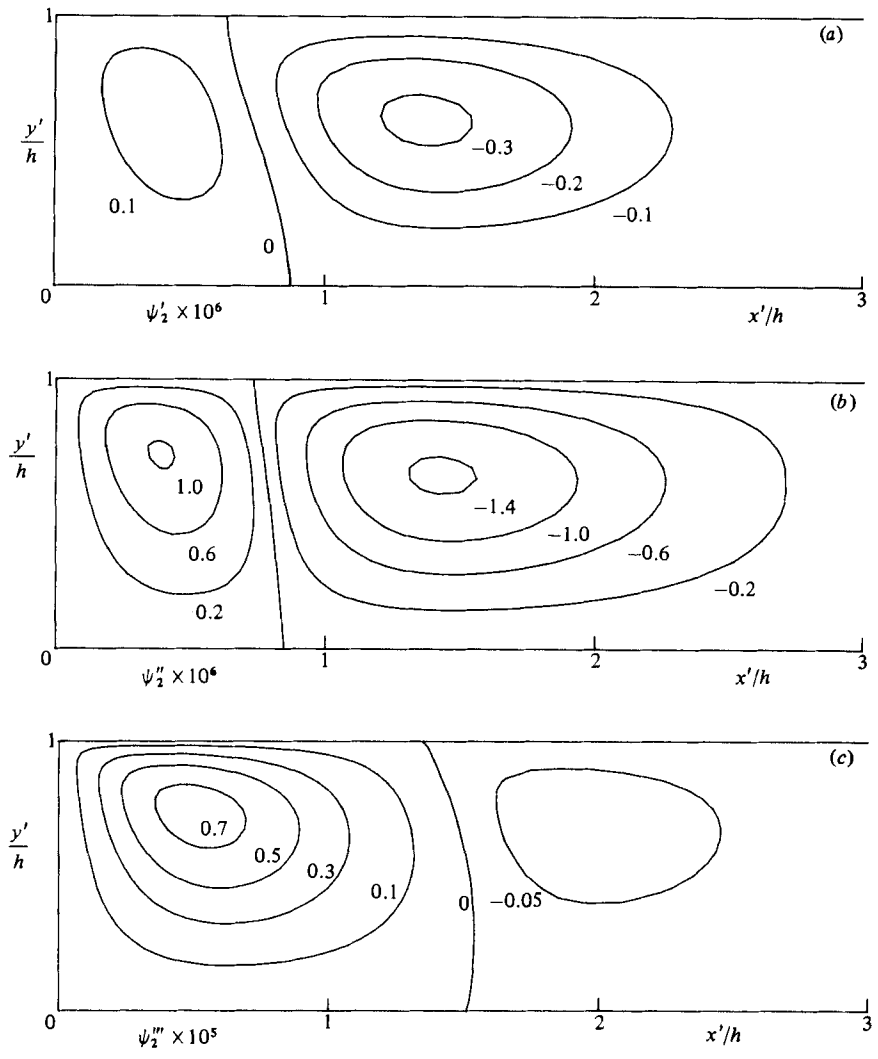

FIGURE 4. $O(A^2)$ correction on stream function: streamlines.

At $O(A^2)$

$$\theta_2^c = -\theta_2^w = \theta_2(\xi, y) = Re\, Pr\, \theta_2'(\xi, y), \tag{3.23a}$$

$$\psi_2^c = \psi_2^w = \psi_2(\xi, y) = Re^2\, \psi_2' + Re^2\, Pr\, \psi_2'' + Re^2\, Pr^2\, \psi_2''', \tag{3.23b}$$

$$c_2 = 0, \quad b_2 = \frac{-1}{120} Re\, Pr. \tag{3.23c}$$

The numerically obtained isolines of θ_2', ψ_2', ψ_2'', ψ_2''' are plotted respectively in figures 3, 4 (a, b, c).

The strong dependence of θ_2' on vertical position clearly indicates a departure from the pure-conduction regime. The gradient $\theta_{2,\xi}'$ is located near the end regions, with opposite signs at the free surface and the bottom of the enclosure. The three components ψ_2', ψ_2'', ψ_2''' give rise to a correction of the same type, that is an upward stream located near $\xi = 1$.

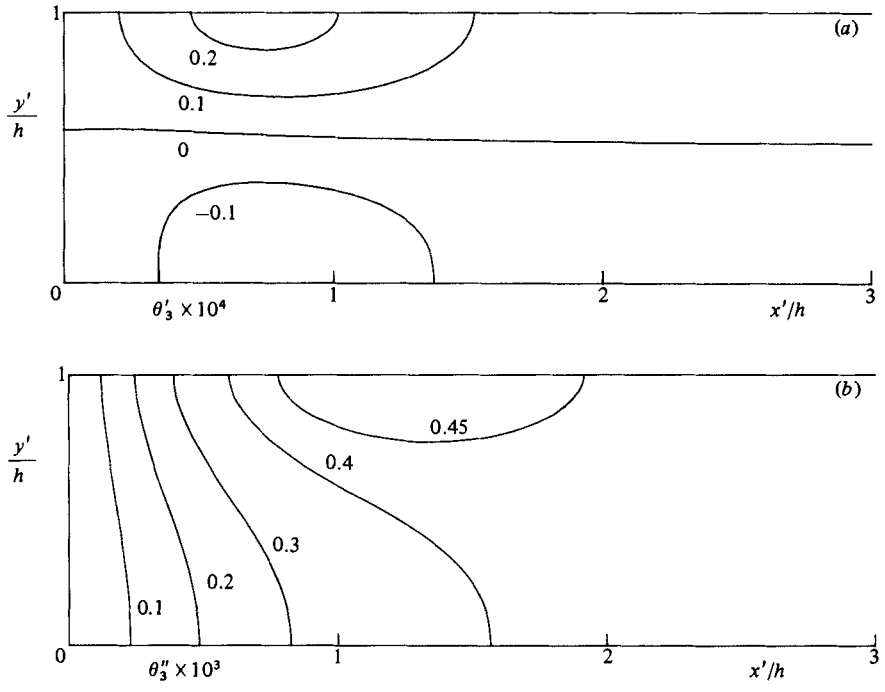

FIGURE 5. $O(A^3)$ temperature correction: isotherms.

At $O(A^3)$

$$\theta_3^{\mathrm{c}} = \theta_3^{\mathrm{w}} = \theta_3(\xi, y) = Re^2\, Pr\, \theta_3' + Re^2\, Pr^2\, \theta_3'', \tag{3.24a}$$

$$b_3 = -\tfrac{1}{2}c_3 = 0.43\ldots \times 10^{-3} Re^2\, Pr^2. \tag{3.24b}$$

The numerically obtained isotherms are plotted respectively in figures 5(*a*, *b*). It may be noticed that both corrections modify the longitudinal temperature gradient only near the endwalls.

At $O(A^4)$

$$\theta_4^{\mathrm{c}} - c_3\,\xi = -(\theta_4^{\mathrm{w}} - c_3\,\xi),$$

and, as a consequence of the corresponding matching conditions,

$$c_4 = 0.$$

The next correction on the core temperature gradient is therefore $O(A^5)$. Owing to the correspondingly high number of numerical solutions, the evaluation of further corrections has not been performed.

3.1.3. *Analysis of the flow-field features.* The expansion for the stream function

$$\psi^{(\mathrm{c,w})} = \psi_0 \pm A\, Re(\psi_1' + Pr\, \psi_1'') + (A\, Re)^2\, (\psi_2^1 + Pr\, \psi_2'' + Pr^2 \psi_2''') + O(A^3) \tag{3.25}$$

and for the temperature gradient

$$T_{,x}^{(\mathrm{c,w})} = \pm \frac{\theta_{,\xi}^{(\mathrm{c,w})}}{A} = 1 \pm A\, Re\, Pr\, \theta_{2,\xi}' + (A\, Re)^2\, (Pr\, \theta_{3,\xi}' + Pr^2\, \theta_{3,\xi}'') + O(A^3) \tag{3.26}$$

(where + and − hold for c and w respectively) obtained by adding the various terms of the end-region solution, describe, owing to the matching conditions, the entire flow field in the cavity. The qualitative features of the above solutions are here discussed.

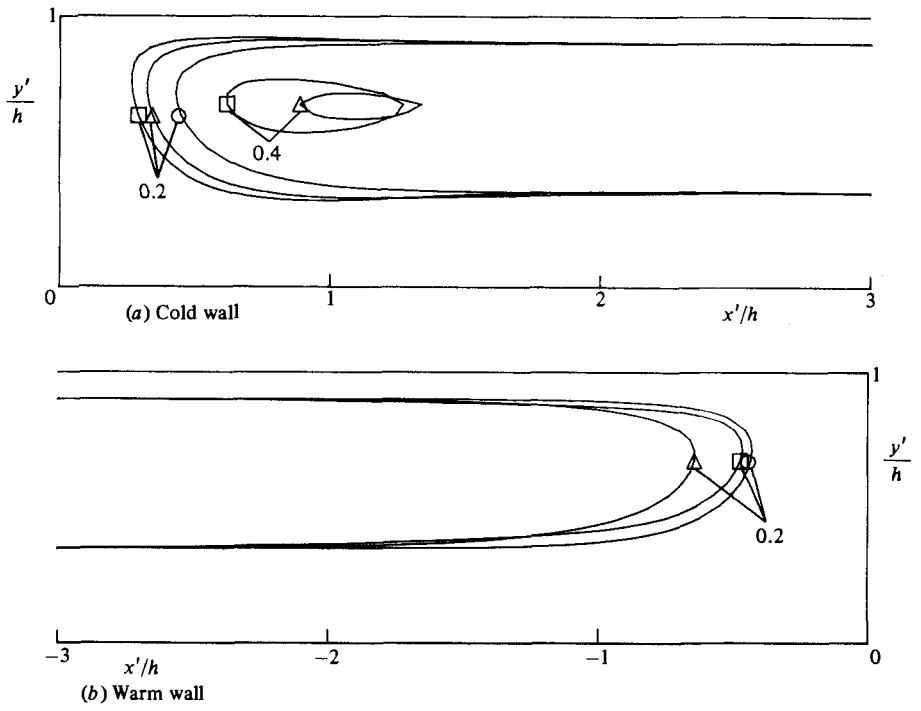

FIGURE 6. Streamlines of the flow field for $Pr = 1$, $A\,Re = 25$: ○, ψ_0; △, $\psi_0 \pm A\,Re(\psi_1' + Pr\,\psi_1'')$; □, $\psi_0 \pm A\,Re(\psi_1' + Pr\,\psi_1'') + (A\,Re)^2(\psi_2' + Pr\,\psi_2'' + Pr^2\,\psi_2''')$.

First it may be observed that, in view of the similar behaviour of ψ_1', ψ_2' and of ψ_2', ψ_2'', ψ_2''', the flow-field qualitative structure is not affected, at least up to $O(A^2)$, by Pr, which only controls the departure of the lateral thermal gradient from pure-conduction-regime value of units.

In figures 6 (a, b) the effect of $O(A\,Re)$ and $O(A^2\,Re^2)$ corrections on ψ_0 are analysed, assuming $Pr = 1$ and $A\,Re = 25$. The $O(A\,Re)$ correction increases the recirculating velocity near the cold wall, while it has an opposite effect near the warm wall. The contributions ψ_1' and ψ_1'', even if qualitatively similar, are due to different physical phenomena. The increase (decrease) of recirculating velocity near the cold (warm) wall, when due to ψ_1', is the first-order consequence of the increasing contribution of inertial with respect to diffusive terms. The similar variation, when due to ψ_1'', is connected to the $O(A\,Re)$ increase (decrease) of the temperature gradient at the free surface near the cold (warm) wall, and hence of the local driving force. The local variation of the temperature gradient is, in turn, due to the increasing contribution of convective terms in the temperature diffusion equation.

In a similar way the effect of the $O(A^2\,Re^2)$ corrections could be explained, accounting for the mixed convection of vorticities ω_0, ω_1 along the flow field ψ_0, ψ_1, and for the local variation of the driving force owing to the $O(A^2\,Re^2)$ correction on the temperature gradient.

The combined effect of $O(A\,Re)$ and $O(A^2\,Re^2)$ corrections may thus give rise, especially near the cold wall, to locally closed streamlines, as shown in figure 6(a). Moreover, one can recognize a tendency for the horizontal scale of the regions near the endwalls to decrease, with a corresponding increase in the recirculating velocity. This trend for increasing values of $A\,Re$ is consistent with the endwall boundary-

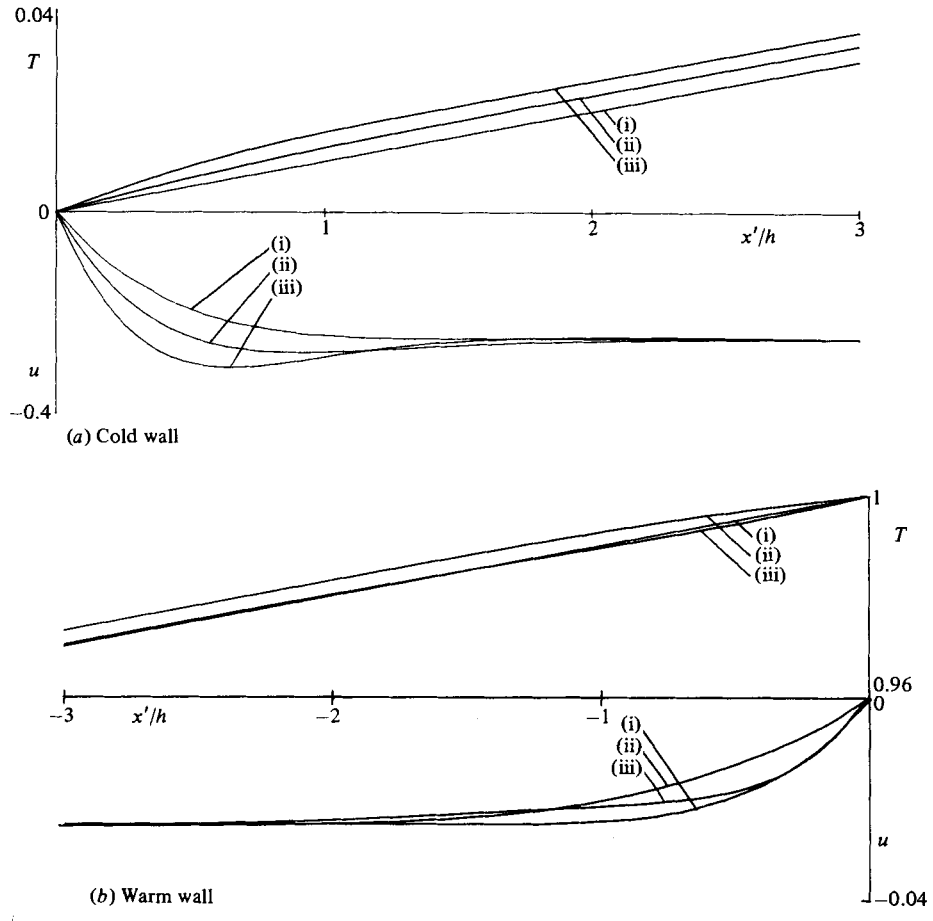

FIGURE 7. Surface temperature and velocity profiles of the flow field for $Pr = 1$, $A\,Re = 25$, $A = 0.01$. The plots (i), (ii) and (iii) correspond respectively to the $O(1)$, $O(A)$ and $O(A^2)$ estimates of surface velocity or temperature.

layer-type structure that characterizes the flow, as shown in §4, for large values of $A\,Re$.

The effect on the temperature gradient along the free surface is shown in figures 7 (*a*, *b*). The $O(A\,Re)$ correction gives rise to a local increase (decrease) of the horizontal temperature gradient, near the cold (warm) wall, while as a consequence of the $O(A^2\,Re^2)$ correction the temperature gradient first increases and then decreases, away from both endwalls.

The resulting increase with $A\,Re$ of the longitudinal temperature gradient near the end walls is consistent with the development there of thermal boundary layers, as shown by the numerical solutions in §4.

As a further result of the asymptotic theory the correlation between the Nusselt number, that is the non-dimensional value of the longitudinal heat flux at the cold wall, and Re, Pr, A may be evaluated. By definition

$$Nu = \frac{\int_0^h \lambda \left.\frac{\partial T'_c}{\partial x'}\right|_{x'=0} dy'}{\lambda(T'_w - T'_c)\,A} = \int_0^1 \left.\frac{\partial T_c}{\partial x}\right|_{x=0} dy, \tag{3.27}$$

and, on account of (3.26),

$$Nu = 1 + A\,Re\,Pr \int_0^1 \theta'_{2,\xi}\,d\xi + A^2 Re^2 \left(Pr \int_0^1 \theta'_{3,\xi}\,dy + Pr^2 \int_0^1 \theta''_{3,\xi}\,dy \right) + O(A^3). \quad (3.28)$$

The corrections θ'_2 and θ'_3 do not contribute to the heat flux, since it can be shown that

$$\frac{d}{d\xi}\left(\int_0^1 \theta'_2\,dy \right) = \frac{d}{d\xi}\left(\int_0^1 \theta'_3\,dy \right) = 0.$$

Hence, from a numerical integration along y, for $\xi = 0$, of the $\theta''_{3,\xi}$ distribution, it follows that

$$Nu = 1 + 5.96 \times 10^{-4} A^2 Re^2 Pr^2 + O(A^3), \quad (3.29)$$

which gives the first correction to the pure-conduction value $Nu = 1$. This result may be used as a further illustration of the difference between a pure-conduction limit for $Re \to 0$ with A fixed, and the present asymptotic expansion where $Nu = 1$ may be achieved even for large values of Re and Pr, provided that A is sufficiently small.

3.2. *Ranges of validity of the asymptotic solution*

From a mathematical point of view a convergence criterion should be developed to determine, for given values of Pr and Re, the range of A where the present asymptotic solution holds. Even if a rigorous convergence criterion is not obtained, it is possible to determine the range of values of A and Cr where the illustrated results may be of practical use.

First the numerical solutions for ψ_0, ω_0 near the endwalls show that streamlines as well as equivorticity lines are parallel to the ξ-axis for $\xi \geqslant 2$. Thus the parallel flow in the central core can be established if

$$A \lesssim 0.25. \quad (3.30)$$

Moreover, Re and Pr will be chosen in such a way that higher-order terms in the asymptotic expansions are small with regard to the first: if 0.1 is taken to be small relative to 1 it is found that the following conditions must be satisfied

$$A\,Re \lesssim 10^2, \quad (3.31)$$

$$A^2 Re^2 Pr^2 \lesssim 10^3. \quad (3.32)$$

On account of the above conditions and of the values obtained for c_k, b_k the temperature gradient in the central core, given by (3.15),

$$K_1 = 1 - 0.86\ldots \times 10^{-3}\,Re^2 Pr^2 A^3 + O(A^3) \quad (3.33)$$

is found to be dominated by the first term. This confirms the present solution to be a proper model of the thermocapillary flow when pure conduction is the dominant mechanism of the heat-transfer process.

Finally, in order to evaluate the range for Cr, the free surface $O(Cr)$ correction is evaluated. By a straightforward application of the domain perturbation method, (3.5d) gives at $O(Cr)$

$$A\,H^{[1]}_{,xx} + [p^{[0]} - 2v^{[0]}_{,y}]_{y_0=1} = 0.$$

Hence, in the core region where $v^{[0]} = 0$ and $p^{[0]} = -\frac{3}{2}(K_1/A)\,(x - C)$,

$$H^{[1]}_{,xx} = \frac{3}{2}\frac{K_1}{A^2}(x - C); \quad (3.34)$$

that is $H^{[1]} = 1/O(A^2)$ as $A \to 0$. Hence, by setting $H^{[1]} = \overline{H}^{[1]}/A^2$ we get

$$H = 1 + \frac{\overline{H}^{[1]}_{(x)}}{A^2} Cr. \tag{3.35}$$

Equation (3.35) shows that, if we want the $O(A^n)$ expansion of the zeroth-order solution $\psi^{[0]}$, $T^{[0]}$ to be an approximate evaluation of the flow field, it must be

$$Cr = O(A^{n+3}). \tag{3.36}$$

In particular, for $n = 0$, $Cr = O(A^3)$, as assumed by Sen & Davis (1982). It may be observed that, under this condition, (3.35), accounting for (3.34), gives a first-order correction on the free-surface shape that corresponds to the one given by equation (4.27) of Sen & Davis.

If condition (3.36) is not satisfied, the computation of higher-order terms for the expansion (3.7) in Cr is required. This can be done, in principle, by a numerical integration of the differential systems that result, at $O(Cr^n)$, from the domain perturbation technique. On the other hand it may be shown that, by setting $Cr = \overline{C}A^3$, an expansion in A of the various orders in Cr may be performed. In this case (3.7) gives an expansion in A which may be reduced to the one proposed by Sen & Davis.

Since the main purpose of the present work is a preliminary analysis of the trends of the thermocapillary flow field at increasing Reynolds numbers, which, at least for moderate values of Cr and contact angles nearly equal to $\frac{1}{2}\pi$, seem to be scarcely affected by the free-surface deformation, no attempt has here been made to evaluate the $O(Cr)$ flow field.

The rough estimates of the ranges of validity here mentioned will be checked and discussed later in §4 in comparison with the numerical results.

4. Numerical results

4.1. *Computational model*

The main features of the computational procedure, described in detail in Strani & Piva (1982), are here briefly recalled for the sake of completeness.

For the finite-difference integration of the bulk conservation equations (2.1)–(2.4) the field variables u^k, p and T are localized, in the transformed plane, on independent meshes shifted with respect to a reference cell, to reproduce the proper extension of the MAC method (Harlow & Welch 1965) to curvilinear coordinates (Piva, Di Carlo & Guj 1980). In particular, the contravariant velocity components, directly connected to the mass fluxes across the cell sides, are located at the cell midsides, while the pressure and temperature are located at the centre of the cell.

The metric coefficients, associated with all variables in the equations, need to be calculated both at the centre of the cell and at the cell midsides, that is in a grid twice as fine as the one adopted for the physical variables. The momentum- and energy-conservation equations for the fluid bulk are integrated by a standard time-dependent-like iterative procedure which satisfies, at each time step, the mass-conservation equation up to a certain level with successive iterations over a simplified set of equations (Hirt & Cook 1972). The boundary values of the field variables are obtained, at each iteration step, by a finite-difference approximation of (2.8*a*, *c*, *d*), and (2.11). Finally, at each time step, the geometrical configuration $H(x)$ of the interface, consistent with the approximate flow field, is determined by the integration of (2.8*b*) through a semi-analytical technique, described in Strani & Piva (1982).

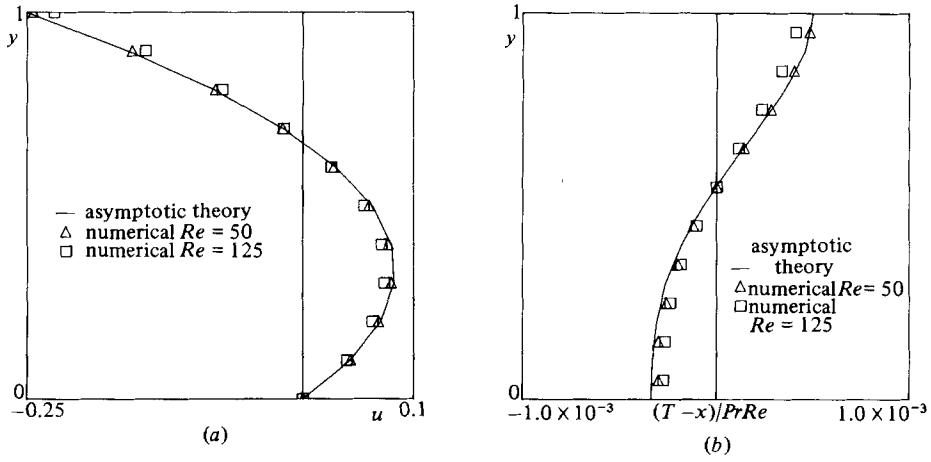

FIGURE 8. u-velocity (a) and temperature (b) profiles in the core, $Cr = 0$, $A = 0.2$. Comparison with the asymptotic theory.

The numerical calculations, for the lower Reynolds numbers, have been performed on a 20×10 or 10×20 regular mesh, depending on the value of the aspect ratio of the cavity. Locally finer meshes have been adopted by an appropriate choice of the streching functions in (2.5a) and (2.5b), to increase the numerical resolution in the lateral regions where strong temperature and velocity gradients occur at large Reynolds numbers. In these conditions an upwind finite-difference scheme has also been used for the convective terms. Finally, a constant Prandtl number, $Pr = 1$, has been assumed in the calculations.

4.2. *Comparison with the asymptotic theory*

Let us consider first the flow field in a shallow cavity, that is a cavity with an aspect ratio $A \to 0$, as required by the asymptotic theory developed in §3.

An aspect ratio $A = 0.2$ sufficiently small to satisfy the required condition of validity ($A \lesssim 0.25$) for the asymptotic theory, but large enough to keep the computer effort reasonably low, has been considered for the numerical solutions. A zero crispation number and a $\frac{1}{2}\pi$ value of the contact angle at the lateral walls have been also assumed in a first set of numerical solutions in order to match the hypothesis, assumed in §3, of negligible surface deformation.

The computed flow field presents the same general characteristics illustrated in §3, at values of the Reynolds numbers which satisfy the upper bounds $ARe < 10^2$ and $A^2Re^2Pr^2 < 10^3$ for the asymptotic expansions truncated at second order to be valid. A parallel flow dominates the central part of the flow field, while the lateral recirculations are confined in two $O(A)$ layers near the cavity walls. The $u_2 = u$ velocity and temperature profiles along the normal to the free surface in the central section of the enclosure (figure 8) are in perfect agreement with the corresponding theoretical core solutions (3.14), (3.15) shown on the same figure.

The surface temperature distribution (figure 9, $Re = 50$) clearly shows the prevailing effect of the first-order correction θ_1 on the pure-conduction regime θ_0, that is a symmetric temperature increase over the linear distribution, whose gradient is concentrated near the endwalls (figure 7). The second-order temperature correction θ_2, which is antisymmetric – producing an increase (decrease) of the temperature

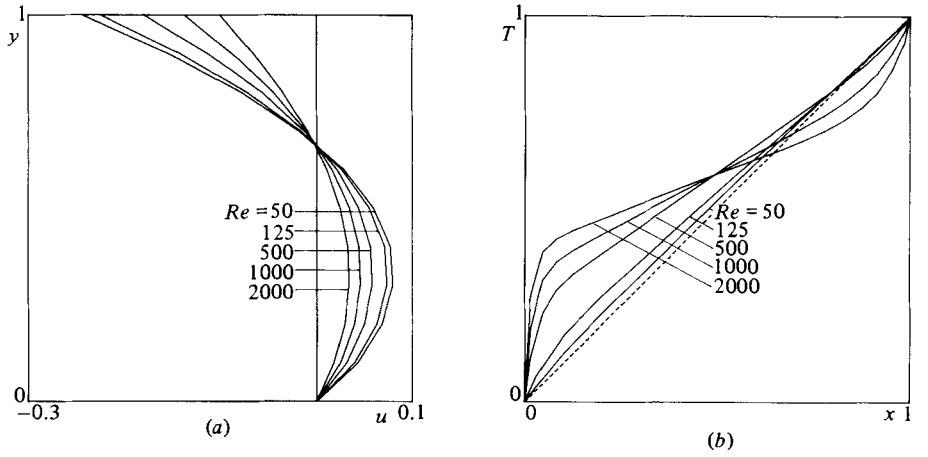

FIGURE 9. u-velocity profiles in the central region (a) and surface temperature distribution (b) for increasing values of Re; $Cr = 0$, $A = 0.2$.

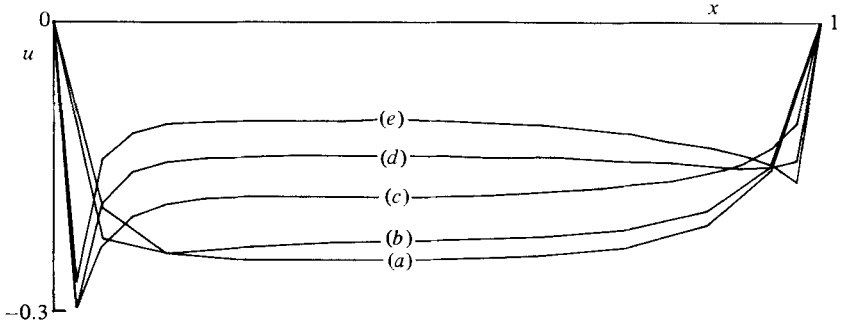

FIGURE 10. Surface velocity distribution for increasing values of Re; $Cr = 0$, $A = 0.2$: (a) $Re = 50$; (b) 125; (c) 500; (d) 1000; (e) 2000.

gradient near the cold (hot) wall – has a significant, but still small, effect at the Reynolds-number value under consideration.

Analogously the surface velocity distribution (figure 10, $Re = 50$) is essentially given by the zeroth-order solution ψ_0, corresponding to the first-order temperature correction θ_1, with a weak effect of the first-order correction ψ_1, which is in turn induced by the second-order temperature correction θ_2.

Very good agreement with the asymptotic solution is found even for $Re = 125$, which is near the upper limit of validity of theoretical results. The effect of the second-order temperature correction θ_2 on the surface temperature distribution now becomes significant, and gives temperatures even lower than pure conduction near the warm wall (figure 9, $Re = 125$). Consistently the first-order solution ψ_1 modifies the surface velocity distribution (figure 10, $Re = 125$). The appearance of the second-order correction ψ_2, which tends to give boundary-layer-type flows near the endwalls (see figure 7), can also be observed, but it will be more evident for larger Reynolds numbers.

The comparison between theoretical and numerical results for Re larger than the limit of validity may be performed only by analysing some characteristic or global

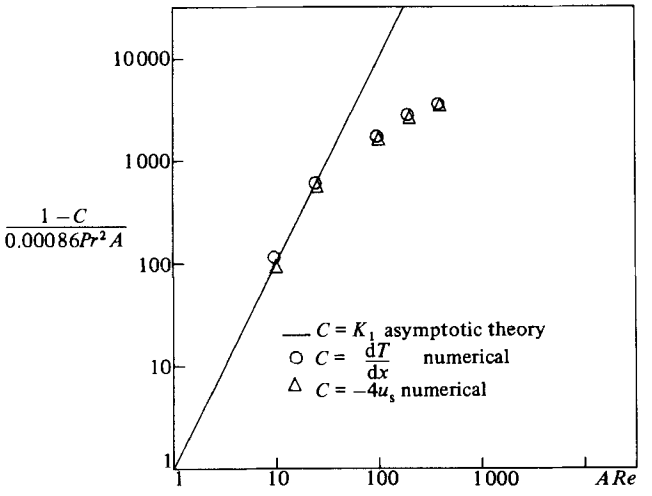

FIGURE 11. Surface velocity and temperature gradient in the core region as a function of ARe, with $Cr = 0$, $A = 0.2$.

quantities of the flow field. In particular, let us consider the surface value of the u-velocity or the related temperature gradient in the core region.

From (3.14) and (3.15) the asymptotic theory gives for these quantities

$$-4u_s = \left(\frac{\partial T}{\partial x}\right)_s = K_1, \tag{4.1}$$

which, in turn, assumes the form (3.33) discussed in §3. The analytical and the numerical results for the above two quantities are plotted as functions of ARe (for $A = 0.2$) on a logarithmic scale in figure 11. The analytical expression matches the numerical results perfectly up to $Re \approx 125$ (that is, approximately the presumed limit of validity of the theory) and clearly diverges for increasing Re, as the influence of higher-order terms becomes larger in the theoretical solution.

An analogous behaviour is shown by the Nusselt number, which accounts for the global heat transfer along the cavity. The analytical expression (3.29) given by the asymptotic theory is compared in figure 12 with the numerical results. The diagram shows a fair agreement up to the mentioned limit of $Re \approx 125$, considering that in 3.29 the error is $O(A^3)$ ant not $O(A^5)$ as for the expression (3.33).

4.3. *Effect of free-surface deformation*

If the hypothesis of zero crispation number, considered in §4.2, is removed, the free surface is allowed to move during the transient motion and to assume a deformed configuration, with respect to the rectilinear one, at steady-state conditions.

The case $A = 0.2$, $Re = 125$ discussed in §4.2 for $Cr = 0$, has been considered here again for a relatively large value of the crispation ($Cr = 0.1$), to emphasize the surface deformation and its influence on the bulk flow field.

The function $H(x)$, which provides the free-surface shape through the numerical calculations, is plotted in figure 13 together with the theoretical $O(Cr)$ estimate given by (3.34). The agreement between the theoretical and the numerical values is very satisfactory, at least for cases in which the deformation of the surface is not too large.

The surface temperature and velocity distributions, in comparison with those

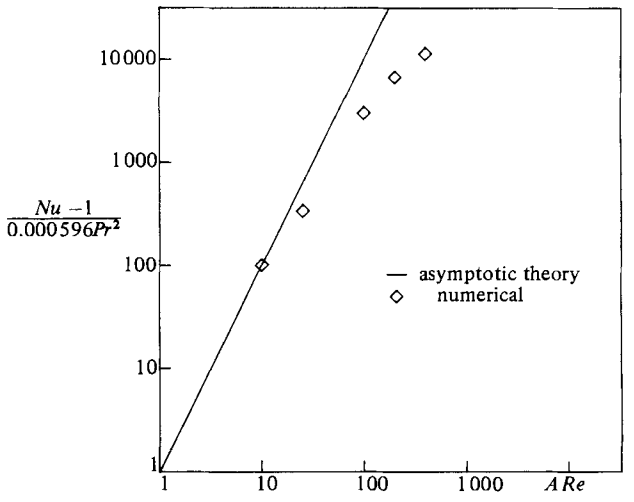

FIGURE 12. Nusselt number as function of ARe, with $Cr = 0$, $A = 0.2$.

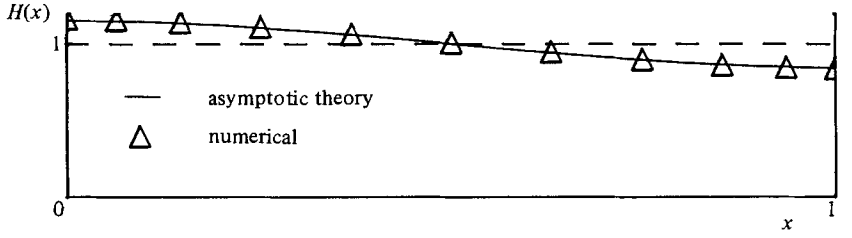

FIGURE 13. Free-surface configuration when $Cr = 0.1$, $A = 0.2$, $Re = 125$; comparison of numerical results with the asymptotic theory.

previously obtained for $Cr = 0$, are plotted in figures 14(a, b). The differences in the temperature profiles seem to be negligible, while the modified form of the surface velocity suggests that a core-region solution based on a local value of A might be acceptable. The small influence of the free-surface deformation on the structure of the flow field is confirmed for larger values of A and Re.

4.4. *The boundary-layer-type flow near the lateral walls*

At larger Reynolds numbers, for $A = 0.2$, a central region of parallel flow is still present. The corresponding u-velocity profile normal to the free surface (figure 9a) maintains, for increasing values of Re, the characteristic shape given by the core solution of the asymptotic theory. In particular, the depth of the velocity inversion point with respect to the free surface stays constant, at the value given by the asymptotic theory. However, the value of the maximum velocity at the free surface decreases for increasing Re, owing to the corresponding decrease of the surface temperature gradient, and hence of the driving force, in the core region. Consistently with the increasing influence of the convection terms, the surface temperature gradients near the lateral walls, particularly near the cold wall, increase with Re, as shown by the surface temperature distribution up to $Re = 2000$ (figure 9b).

The larger surface temperature gradient near the cold wall develops a local increase in the driving force. This leads to a quite complex stagnation flow field, with a

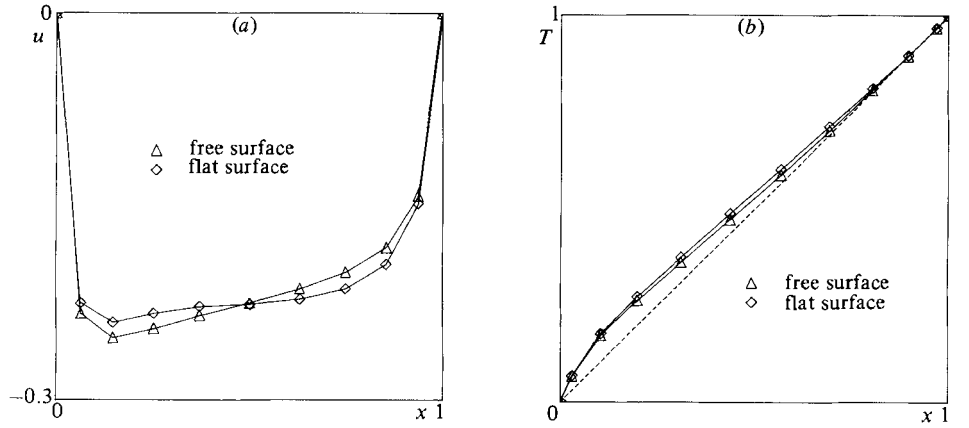

FIGURE 14. Effect of free-surface configuration on surface velocity (*a*) and temperature (*b*); $A = 0.2$, $Re = 125$.

significant acceleration near the wall, positive first, up to the maximum velocity, and negative afterwards to meet the zero-velocity boundary condition. A boundary-layer-type flow grows downwards along the cold wall, starting from the stagnation point at the surface. The flow near the hot wall has a similar behaviour, but it is less dramatic because the velocity is in the opposite direction with respect to the wall. In fact, the lower temperature gradient that develops on the hot side requires a larger Re to generate a local maximum in the surface velocity distribution, as clearly shown by the surface-velocity diagrams (figure 10) up to $Re = 2000$.

In corresponding to the two relative maxima in the surface velocity profile, two stream-function maxima appear in the field at $Re = 2000$, while for lower Re the maximum is located close to the central section. This behaviour, which is consistent with the trend predicted by the asymptotic theory for increasing Re, is analogous to the one that occurs in natural convection flow fields at increasing Grashof numbers (Cormack *et al.* 1974).

4.5. *Effect of the aspect ratio*

The condition of small aspect ratio, required in §4.4 for comparison with the theoretical results, is here removed to investigate the structure of the flow field in a cavity with characteristic dimensions h and l of the same order. Hence a value of $A = 1$ (that is a square cavity) has been assumed first, together with a value $Cr = 0$, to study the behaviour of the flow field for a range of Re from 10 to 2×10^3.

The u-velocity profile along the normal to the free surface at the central section (figure 15*a*) maintains a similar form, for this entire range of Re, as in the core region of the shallow cavity. The surface temperature distribution (figure 15*b*) shows the tendency, already discussed for $A = 0.2$, to localize, for large Re, the temperature gradient near the lateral walls and in particular near the cold wall. Consistent with such temperature gradients (that is driving forces) the surface velocity distribution (figure 16) shows a concentrated growth, at increasing Re, first near the cold wall and later near the hot wall too.

While for low Re the entire field strongly 'feels' the presence of the lateral walls – that is, the flow cannot be subdivided into different regions as for $A \to 0$ – at larger Re a central core region develops. In this central region the temperature gradient assumes very small values and the surface velocity becomes approximately

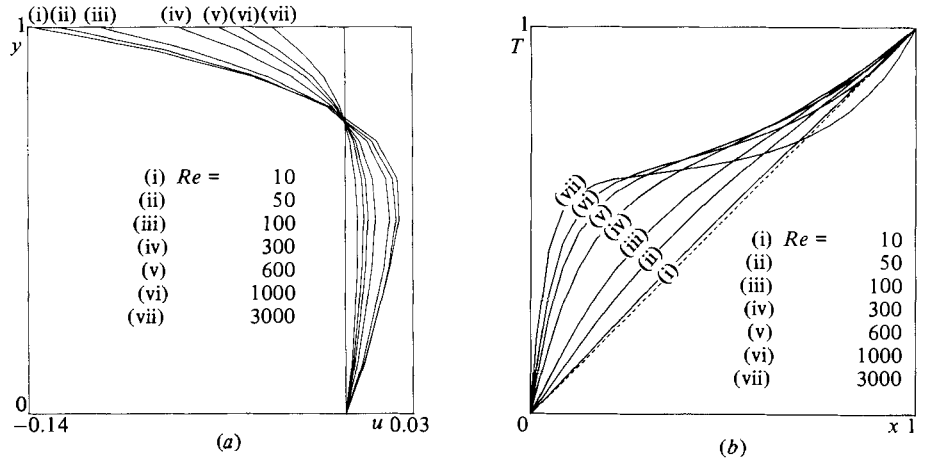

FIGURE 15. u-velocity profiles in the central region (a) and surface temperature distribution (b) for increasing values of Re, with $Cr = 0$, $A = 1$.

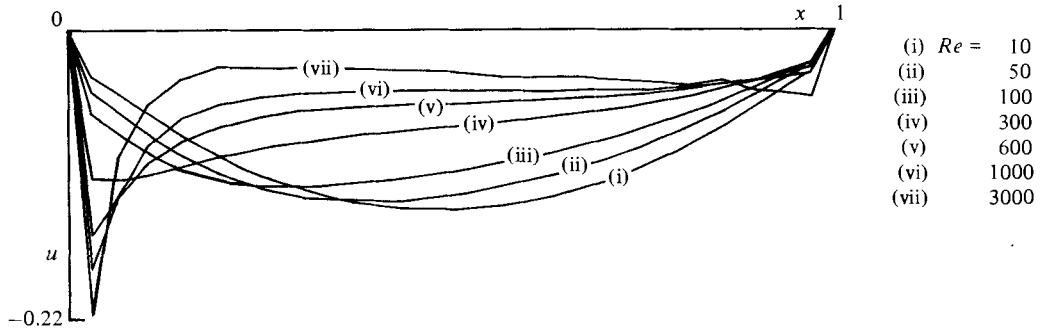

FIGURE 16. Surface velocity distribution for increasing values of Re; $Cr = 0$, $A = 1$.

constant, giving rise to a quite-parallel flow, as in the shallow cavity. The depth d/h of the velocity inversion, with respect to the free surface, in the central region (see figure 15a) is slightly smaller than for $A = 0.2$, but, as in the previous case, it is quite independent of Re.

A narrow cavity, with a large aspect ratio ($A = 5$) has also been considered in order to determine whether the main features of the flow-field structure, described above, are still maintained under these conditions. Considering the relatively small effect of the surface deformation on the flow field, a zero crispation number is assumed, while a range of Re from 10^2 to 2.5×10^3 is now considered.

The velocity profiles along the normal to the free surface at the central section (figure 17a) maintain a characteristic self-similar structure for the entire range of Re, as for $A = 0.2$ and $A = 1$. Their shape, however, differs from the previous cases, the fluid motion now being significant only in the upper part of the field. In fact the velocity goes approximately to zero in a depth of the order of l – nearly $\frac{3}{2}l$ – while very weak recirculations appear in the remaining part of the flow field. The surface temperature profiles at the corresponding values of Re are shown in figure 17(b).

The depth of the velocity inversion with respect to the free surface maintains, in the central section, a value of approximately $\frac{1}{18}h$, quite independent of Re (at least for the range considered). As just analysed for the square cavity, at increasing Re,

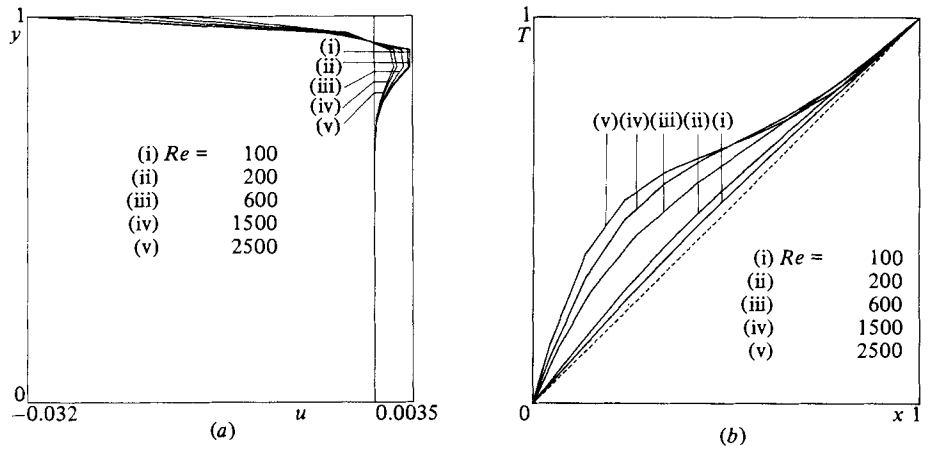

FIGURE 17. u-velocity profiles in the central region (a) and surface temperature distribution (b) for increasing values of Re; $Cr = 0$, $A = 5$.

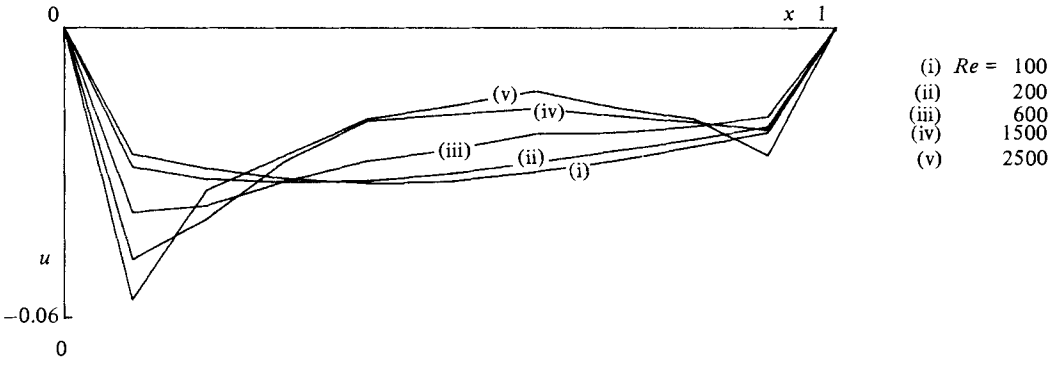

FIGURE 18. Surface velocity distribution for increasing Re; $Cr = 0$, $A = 5$.

a central region with a low temperature gradient develops, and the surface velocity tends to become approximately constant there (figure 18), generating a core region of quasiparallel flow.

5. General considerations on the flow-field structure

The numerical results described in the previous sections for three substantially different values of the aspect ratio give insight into some general characteristics of the flow-field structure. The surface-tension gradient, acting as a driving force, accelerates the bulk fluid in a layer near the free surface itself. The backflow in the remaining part of the cavity gives a maximum of the stream functions at a small depth under the free surface. At the central section $x' = \frac{1}{2}l$ the inversion depth d/l of the non-dimensional u-velocity increases with A, but is quite independent of Re over the entire range considered for the numerical results, as shown by the u-velocity profiles in figures 9(a), 15(a) and 17(a) respectively for $A = 0.2$, 1 and 5. The surface tangential balance at $x' = \frac{1}{2}l$ requires that

$$\mu \frac{u'_{\text{core}}}{d} = \left|\frac{\mathrm{d}\sigma'}{\mathrm{d}T'}\right|_{T'_c} \frac{(\Delta T)_{\text{core}}}{l}. \tag{5.1}$$

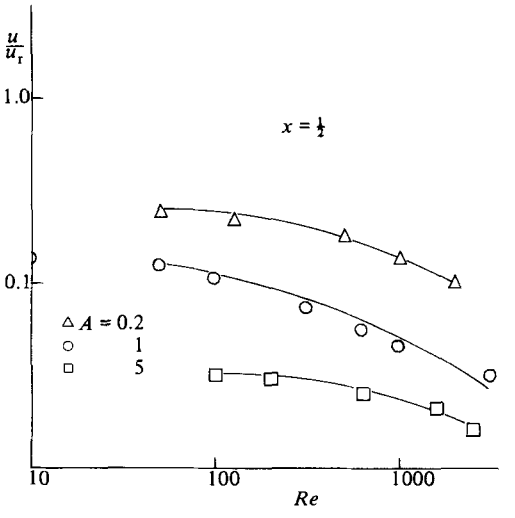

FIGURE 19. Non-dimensional velocity at the central section $x' = \frac{1}{2}l$ as a function of Re; $Cr = 0$.

For d/l approximately constant, the decrease of the surface velocity with Re in the central core region (figure 19), is merely due to the decrease, in the same region, of the surface temperature gradient, shown in figures 9(*b*), 15(*b*) and 17(*b*). The parallelism between the surface-velocity plots for the three different values of the aspect ratio occurs because both d/l and $(\Delta T)_{\text{core}}/l$ depend on A for a given Re. Therefore in the central region the surface layer, in a cavity with imposed temperature differences between the lateral walls and Prandtl numbers of the order of unity, never reaches the transition to boundary-layer-type flow predicted by Ostrach (1982). Very small Prandtl numbers may, however, significantly modify the above behaviour, as will be discussed below.

Approaching the cold wall, the surface layer generates a stagnation flow field which feeds the recirculating lateral region and the backflow towards the hot wall. At increasing values of the ratio between convective and diffusive terms a singular behaviour of the temperature field appears near the cold wall. The growing temperature gradient influences in turn the surface stream velocity, which reaches a peak very close to the cold wall and suddenly decreases to zero, to satisfy the wall boundary condition.

A surface boundary layer appears locally at the upper left corner of the enclosure, near the cold wall. However, with respect to Ostrach's (1982) dimensional analysis the appropriate lengthscales in the x' and y' directions are here given respectively by the thermal boundary-layer thickness δ_T at the surface and by the surface-layer thickness δ_u, that is the inversion depth of the u-velocity profile in the section where the surface velocity has a local maximum.

A measure of δ_T/l has been derived from the non-dimensional temperature gradient at the cold wall according to

$$\frac{\delta_T}{l} = \left(\frac{\partial T}{\partial x}\bigg|_{y=1,\, x=0} \right)^{-1}. \tag{5.2}$$

The computed values of δ_T/l, plotted in figure 20, show a regular decrease with Re. The correlation of the numerical results, indicated by the straight lines in the figure, will be discussed below. An analogous decrease with Re of δ_u/l may be observed

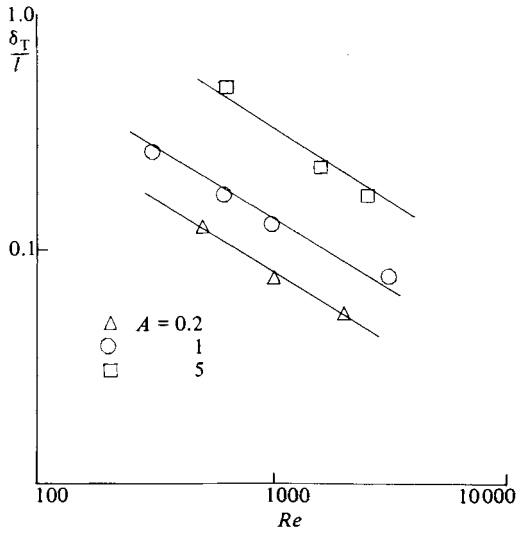

FIGURE 20. Surface thermal boundary-layer thickness δ_T/l as a function of Re.

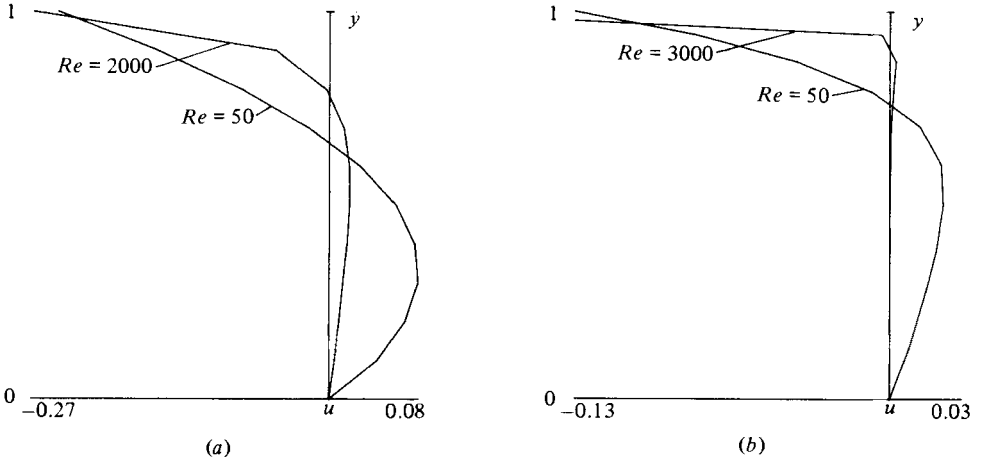

FIGURE 21. u-velocity profiles in the section of maximum surface velocity: (a) $Cr = 0$, $A = 0.2$; (b) $Cr = 0$, $A = 1$.

(figures 21 a, b), for each value of A, by comparing the u-velocity vertical profiles in the section where the maximum surface velocity occurs. It is worth emphasizing that the trends of δ_u/l and δ_T/l, as functions of Re, are strictly interrelated, as can be seen from the inversion-point distribution (figure 22), which appears to be, from the numerical results, quite insensitive to the value of Re. Hence the section of maximum surface velocity seems to get closer to the cold wall, giving a smaller δ_u; much as the thermal boundary-layer thickness δ_T decreases for larger Re.

The maximum surface velocity as a function of Re is plotted in figure 23 for $A = 0.2$, 1 and 5. An asymptotic trend of u'_{max} to constant values both for $Re \to 0$ and $Re \to \infty$ may be observed from the plots. For $Re \to 0$, u'_{max} coincides with the surface velocity at the central section, while a possible explanation of the behaviour for $Re \to \infty$ will be attempted below, through a dimensional analysis.

We must admit at this point that the computed values of δ_T, δ_u and u'_{max} may only

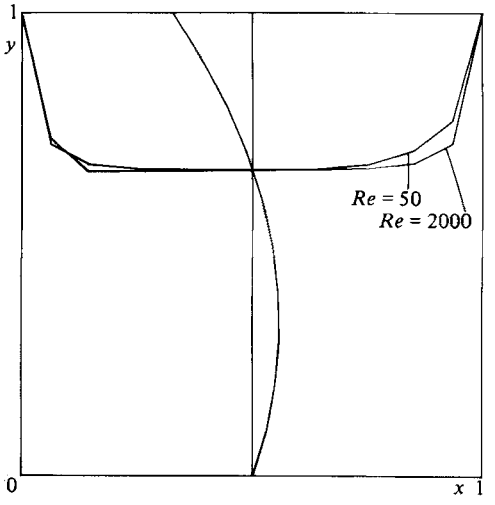

FIGURE 22. Inversion depth of the u-velocity profiles; $Cr = 0$, $A = 0.2$.

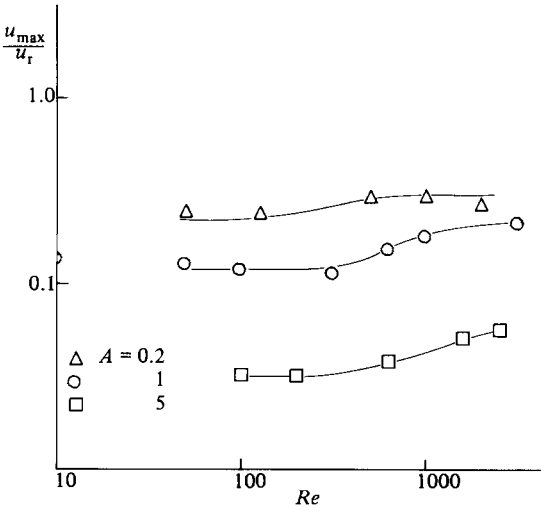

FIGURE 23. Maximum surface velocity as a function of Re.

be used to infer the qualitative tendencies of the flow field for growing Re. In fact, most of the numerical results presented have been obtained at relatively low values of Re – so that the boundary-layer flow near the cold wall is not fully established – while for the higher values of Re, in order to limit computer time, relatively coarse meshes, with corresponding poor accuracy, have been adopted. Nevertheless, the qualitative insight into the structure of the flow field and its transition to boundary-layer-type flow that has been achieved through the numerical simulation may be sufficient to settle a proper dimensional analysis of the flow near the cold wall at large Re.

Thus, if we assume δ_T and δ_u as lengthscales in the x' and y' directions, the surface tangential balance in the section where the maximum velocity occurs yields

$$\mu \frac{u'_{max}}{\delta_u} = \left|\frac{d\sigma'}{dT'}\right|_{T'_c} \frac{T'_w - T'_c}{\delta_T}. \tag{5.3}$$

Moreover, in the boundary-layer region near the cold wall the diffusive and convective terms are assumed to be of the same order of magnitude in the momentum and thermal-energy balances, that is

$$\rho \frac{(u'_{max})^2}{\delta_T} = \mu \frac{u'_{max}}{\delta_u^2}, \tag{5.4}$$

$$u'_{max} \frac{T'_w - T'_c}{\delta_T} = \frac{\mu}{\rho} \frac{1}{Pr} \frac{T'_w - T'_c}{\delta_T^2}. \tag{5.5}$$

By combining (5.3)–(5.5), it follows that

$$\frac{\delta_u}{l} = \frac{A}{RePr}, \tag{5.6}$$

$$\frac{\delta_T}{l} = \frac{A}{RePr^{\frac{1}{2}}} = \frac{\delta_u}{l} \frac{1}{Pr^{\frac{1}{2}}}, \tag{5.7}$$

$$\frac{u'_{max}}{u'_r} = u_{max} = \frac{Pr^{\frac{1}{2}}}{A}. \tag{5.8}$$

It is interesting to note that the thermal boundary-layer thickness given by (5.7) coincides with the expression that follows from the classical stagnation-flow solution (Schlichting 1960), provided that the maximum velocity (5.3) is assumed as the external velocity. Equation (5.7) gives a decrease of δ_T with Re^{-1}, while the correlation of the numerical results (figure 20) is approximated for each value of A by $\delta_T/l = Re^{-\alpha}$ with $\alpha < 1$. The difference in the power-law exponent may be attributed to the numerical overestimation of δ_T/l for increasing Re, owing to the relatively coarse mesh adopted in the computations. Equation (5.8) gives an asymptotic trend of u_{max} to a constant value for $Re \to \infty$, in good qualitative agreement with the same behaviour observed in the correlation of the computed values (figure 23). For $A = 0.2$, and $Re = 2000$, the computed value of u_{max} is clearly underestimated. In this case, in fact, the mesh seems to be too coarse near the cold wall to reach the station where the maximum velocity occurs. The above dimensional analysis is physically consistent for values of the Prandtl numbers that are not too small. In fact, for $Pr \to 0$ the conduction terms prevail over the convection ones, in the entire range of Re, so that the lengthscale in the y' direction remains l and a surface boundary-layer flow may also be established in the central region of the enclosure for increasing Re. In this case the results of the dimensional analysis obtained by Ostrach (1982), with the assumption of a constant longitudinal temperature gradient, maintain their validity.

A better knowledge of the temperature field, when the convective heat transfer is significant, may be achieved by observing the isothermal lines for the values of A considered in the calculations. For $A = 0.2$ and $Re = 2000$ the thermal field is approximately centrosymmetric (figure 24*b*), and two boundary layers are present respectively at the upper left corner and at the lower right corner of the enclosure, resembling, for this feature, a natural-convection flow field. The corresponding surface and bottom temperature profiles are shown in figure 24(*a*). For $A = 1$, $Re = 3000$ the isothermal-line field (figure 24*d*) loses the symmetrical feature, and a thermal boundary layer develops only at the upper left corner, as confirmed by the corresponding surface and bottom temperature profiles (figure 24*c*).

For $A = 5$, $Re = 2500$ the isothermal-line field (figure 24*f*) in the upper part of the cavity maintains the characteristics described for $A = 1$, while in the lower part the isotherms tend to become parallel to the lateral walls as for a pure-conduction thermal field. The bottom temperature profile (figure 24*e*) is, in fact, given approximately by a linear distribution. The tendency of the isothermal lines to become horizontal in the central region of the enclosure for natural convection at large Grashof numbers is partially experienced also in thermocapillary convection for very small values of the aspect ratio, while for increasing A the convective flow remains confined in the upper part of the field near the free surface.

A quantitative analysis of the above features may be performed by considering the average Nusselt number, which accounts for the heat transfer through the enclosure. The average Nusselt number, computed at the lateral walls of the enclosure, is defined by the expression

$$Nu = \int_0^1 \left(\frac{\partial T}{\partial x}\right)_{x=0} \mathrm{d}y, \tag{5.9}$$

which gives $Nu = 1$ for $(\partial T/\partial x)_{x=0} = 1$, that is for pure-conduction heat transfer. The numerical values of Nu as a function of Re are correlated in figure 25 for each of the considered values of the aspect ratio. For shallow cavities, at a fixed Re, the value of Nu increases with A (as in natural convection), as confirmed by the asymptotic theory and by the present numerical results, at least up to $A = 0.2$, while the thermal field approaches the pure-conduction regime, that is $Nu \to 1$, for $A \to 0$.

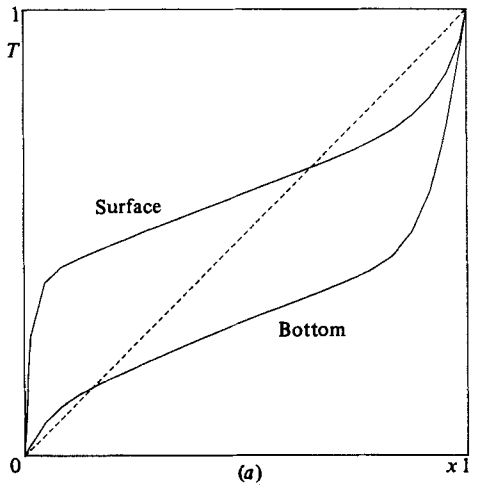

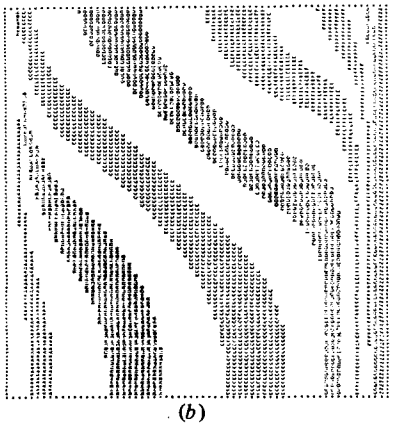

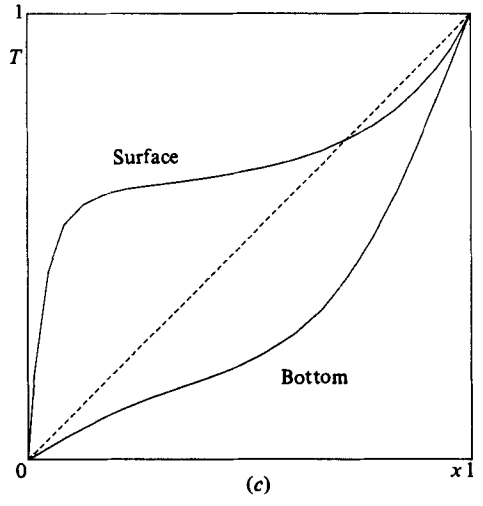

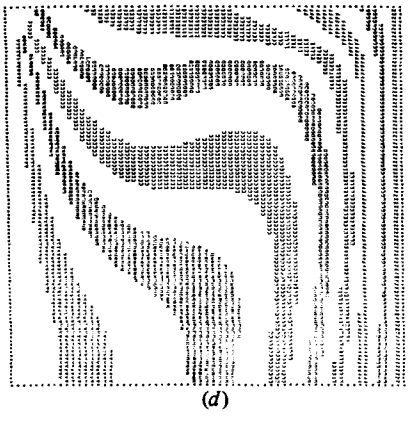

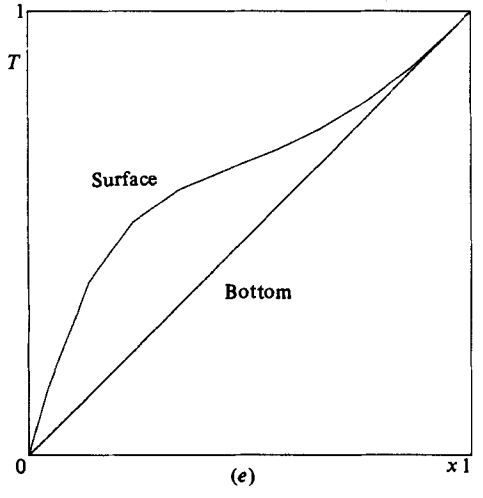

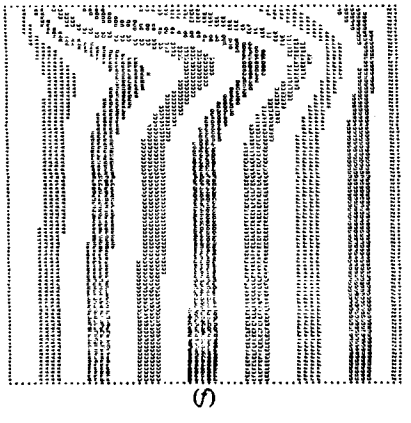

FIGURE 24. Surface and bottom temperature profiles: (*a*) $Cr = 0$, $A = 0.2$, $Re = 2000$; (*c*) $A = 1$, $Re = 3000$; (*e*) $A = 5$, $Re = 2500$. Isothermal-line computer plot: (*b*) $Cr = 0$, $A = 0.2$, $Re = 2000$; (*d*) $A = 1$, $Re = 3000$; (*f*) $A = 5$, $Re = 2500$.

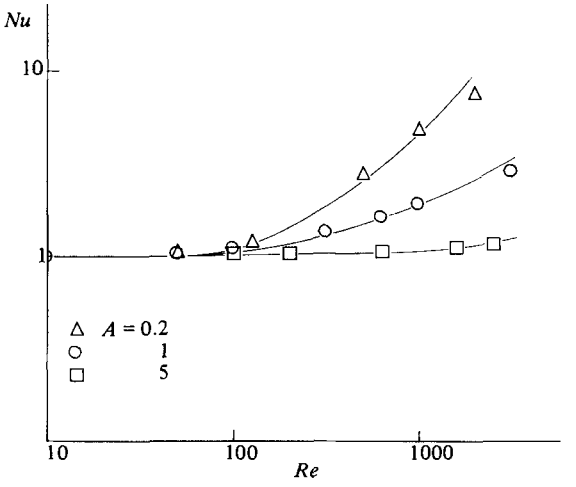

FIGURE 25. Nusselt number as a function of Re.

For narrow cavities, as for $A = 5$, the motion remains confined in a region close to the free surface, as shown by the velocity profiles in figure 17(a), and, as a consequence, a large part of the thermal field is essentially governed by pure conduction. Hence the average Nusselt number tends to unity as $A \to \infty$, in contrast with the behaviour in natural convection, where the average Nusselt number maintains a value approximately independent of A, as stated by Gill (1966). Therefore, in thermocapillary convection the asymptotic tendency to $Nu = 1$, both for $A \to 0$ and for $A \to \infty$, assures the existence of a maximum in the Nusselt number as a function of A.

Some of the described features of the flow-field structure in thermocapillary flows are in good qualitative agreement with the few experimental results achieved with prevailing surface-tension-driven convection. In particular, Schwabe *et al.* (1979) and Chun (1980) give measurements of the surface temperatures in liquid columns, whose distribution presents the characteristic S-shape of figure 15(b). The quantitative differences between the calculated and the measured temperatures – and specifically the lowest (highest) measured values of the temperature gradients near the cold (hot) wall – may be attributed to the presence in the experiments of a relatively large cooling by surface radiation, as previously shown by the numerical simulation of such conditions (see e.g. figure 17 of Graziani, Strani & Piva 1982).

The measurements reported for $A \approx 2$ by Schwabe *et al.* (1979) confirm the observation (see e.g. figure 17a) that the Marangoni convective flow for $A > 1$ is confined in a layer near the free surface. Schwabe & Scharmann (1981) presented also the experimental u-velocity vertical profiles for a plane two-dimensional flow in a $NaNO_3$ melt with $A \approx 0.6$, $Pr \approx 10$ and $Ma \approx 10^5$. A qualitative agreement with the computed velocity profiles in the section of maximum surface velocity (figure 21) may be observed. A quantitative comparison cannot be attempted considering the relevant effect of buoyancy forces and radiation cooling, as seems to be suggested by the location near the hot wall of the maximum surface velocity (Schwabe & Scharmann 1981).

6. Concluding remarks

The numerical results discussed in §5 for $A = 0.2$ and $A = 1$ have shown a small influence of the free-surface deformation on the qualitative structure of the flow field, at least for physically acceptable values of the crispation number ($Cr < 0.5$) and $\frac{1}{2}\pi$ contact angles at the lateral walls. Very large deformations of the free surface may actually occur in technological applications under zero-gravity conditions, for contact angles different from $\frac{1}{2}\pi$, but also in such conditions the main characteristics of the flow field seem to be maintained (Strani & Piva 1982). However, a systematic analysis should be conducted to substantiate the present impression of the relatively small effect of the free-surface displacement.

Moreover, the flow-field structure at large Re needs a deeper investigation based on a more accurate simulation near the lateral walls, in particular the cold one, where a boundary-layer-type flow develops. The above considerations suggest an approach to this analysis, if the hypothesis of $\frac{1}{2}\pi$ contact angle is maintained on the one hand with a simpler mathematical model (e.g. in Cartesian coordinates), but, on the other, with a more sophisticated numerical procedure (e.g. a multigrid technique) permitting, on a locally adaptive mesh, a more accurate solution near the lateral walls. The domain perturbation technique suggested by Joseph & Fosdick (1972), and adopted in §3 in the frame of the asymptotic theory, could hence be applied to determine successive $O(Cr)$ corrections to the flow field, avoiding in this way the two-way coupling between surface configuration and bulk field which is characteristic of the present numerical solutions.

Finally, the surface diffusivity coefficients λ_s, μ_s, whose influence on the overall flow field has been estimated as scarcely significant in a previous study (Piva *et al.* 1981), should be reconsidered in the surface balance equations, at large Re, when very drastic velocity and temperature gradients appear in the surface layer approaching the lateral wall.

REFERENCES

Bedeaux, D., Albano, A. M. & Mazur, P. 1976 *Physica* **82A**, 438.

Bourgeois, S. V. & Brasheors, M. R. 1977 *Prog. Astron. Aero.* **52**, 189.

Chang, C. E. 1978 *J. Crystal Growth* **44**, 168.

Chang, C. E. & Wilcox, W. R. 1976 *Int. J. Heat Mass Transfer* **19**, 355.

Chun, C. H. 1980 *Acta Astronautica* **7**, 479.

Chung, C. H. & Wuest, W. 1978 *Acta Astronautica* **5**, 681.

Clark, P. A. & Wilcox, W. R. 1980 *J. Crystal Growth* **50**, 461.

Cormack, D. E., Leal, L. G. & Imberger, J. 1974*a* *J. Fluid Mech.* **65**, 209.

Cormack, D. E., Leal, L. G. & Seinfeld, J. H. 1974*b* *J. Fluid Mech.* **65**, 231.

Gill, A. E. 1966 *J. Fluid Mech.* **26**, 515.

Graziani, G., Strani, M. & Piva, R. 1982 *Acta Astronautica* **9**, 4.

Harlow, F. W. & Welch, J. E. 1965 *Phys. Fluids*, **8**, 2182.

Hirt, C. W. & Cook, J. L. 1972 *J. Comp. Phys.* **10**.

Joseph, D. D. & Fosdick, R. L. 1972 *Arch. Rat. Mech. Anal.* **49**, 321.

Levich, V. G. 1962 *Physicochemical Hydrodynamics*. Prentice Hall.

Napolitano, L. G. 1978 *Acta Astronautica* **5**, 655.

Ostrach, S. 1982 *Ann. Rev. Fluid Mech.* **14**, 313.

Ostrach, S. & Pradhan, A. 1978 *AIAA J.* **16**, 419.

Piva, R., Di Carlo, A. & Guj, G. 1980 *Comp. & Fluids* **8**.

PIVA, R., STRANI, M. & GRAZIANI, G. 1981 In *Proc. AIDAA VI Natl Congr. Rome.*

SCHLICHTING, H. 1960 *Boundary-Layer Theory.* McGraw-Hill.

SCHWABE, D. 1981 *Physicochem. Hydrodyn.* **2**, 263.

SCHWABE, D. & SCHARMANN, A. 1981 *J. Crystal Growth* **52**, 435.

SCHWABE, D., SCHARMANN, A. & PREISSER, F. 1979 In *Proc. 3rd Euro. Symp. on Material Sciences in Space, Grenoble. ESA* SP-142.

SEN, A. K. & DAVIS, S. H. 1982 *J. Fluid Mech.* **121**, 163.

STRANI, M. & PIVA, R. 1982 *Int. J. Numer. Meth. Fluids* **2**, 367.

STRANI, M., PIVA, R. & GRAZIANI, G. 1982 Thermocapillary convection in a rectangular cavity: part 1, asymptotic theory. *IMA Rep.* 82–5, *Istituto di Meccanica Applicata, Università di Roma.*

YIH, C. S. 1968 *Phys. Fluids* **11**, 477.